International Journal of Heat and Mass Transfer 53 (2010) 2404–2413

Contents lists available at ScienceDirect

International Journal of Heat and Mass Transfer

journal homepage: www.elsevier.com/locate/ijhmt

A numerical simulation for mass transfer through the porous membrane of parallel straight channels

Junfeng Lu [a], Wen-Qiang Lu [b,*]

[a] Technical Institute of Physics & Chemistry of Chinese Academy of Sciences, No. 2 Beiyitiao Street, Zhongguancun, Haidian District, Beijing 100190, PR China
[b] Graduate University of Chinese Academy of Sciences, 19A Yuquanlu, Beijing 100049, PR China

ARTICLE INFO

Article history:
Received 29 October 2009
Received in revised form 19 January 2010
Accepted 22 January 2010
Available online 17 February 2010

Keywords:
Porous plate channel
Porous membrane
Ultra-filtration
Hemodialysis
Reverse osmosis

ABSTRACT

In this paper, by adopting a "half-channel" model, a mass exchange process (presented in the therapy of hemodialysis) between two opposite running flows is numerically simulated. The flows are confined inside channels and separated by intercalary porous membranes. In the simulation, two types of flows, channel flow and ultra-filtration flow, are physically described, respectively, by Navier–Stokes equations and Kedem–Katchalsky (K–K) equations. By further adopting "SimpleR" algorithm, the velocity fields inside the channels are determined, meanwhile, solute mass distributions are predicted by concentration equation. The solid computation in this paper perfectly explored the process of hemodialysis, its results: (1) displayed the flow and solute distribution patterns inside channels; (2) described the ultra-filtration profiles along the surface of the porous membrane; and (3) disclosed an existent nano-scale reverse osmosis problem.

1. Introduction

Filtration process occurs in so many engineering problems. The general method to improve the efficiency of the process is to increase the contact filtration area as while maintain a small volume of a filtration device. Among them, a hollow fiber dialyzer used in the therapy of hemodialysis is a good example. As shown in Fig. 1, inside the dialyzer, the filtration of a substance is through a hollow fiber, of which the wall is made of porous material. Since the fibers are bundled, the whole filtration process is locked inside the small cylindrical device with a diameter of around 5–10 cm and a length of around 50–80 cm. Thus, to study a flow problem like hemodialysis process becomes a typical research to improve filtration efficiency.

Generally, the pore size of the ultra-filtration membrane used in the hemodialysis is in the range from several nano meters to almost several hundred nano meters (Fig. 2) because the size of the metabolic wastes carried by the human blood are ranging across this range. The research in this tiny range is rather important because it discloses the flow behavior that approaches molecular world. During hemodialysis process, to remove different metabolic wastes carried by the blood, the pore size of the membrane is a very important reference. However, mostly, the pores on a membrane surface are non-homogeneous in size (Fig. 2). This diversity sometimes causes solute leaking problem in large size pores and blocking problem in small size pores. So, a homogeneous pore size for a filtration membrane used in ultra-filtration or even conventional filtration process is highly desired because it could cut through the leaking problem of large size solutes. Thus, the simulation in this paper also assumes that the pores on the filtration membrane are homogeneous.

Typically, when studying hemodialysis process, the model [2] shown in Fig. 3 is commonly used. In the model, two fluids with different viscosities are separated by porous membranes. They exchange solute contents through the porous membrane where ultra-filtration occurs. When studying the model shown in Fig. 3, repeating of a structural pattern can be observed between the axes of two channels. With this symmetric property, the "channel model" can be thus further simplified to a "half-channel model"(Fig. 4). In general, flow inside an straight channel can be simply considered as Poiseuille flow (this conclusion already used in tons of numerical literatures and CFD books). However, flow inside a channel formed by nano porous membrane is more complex because the sideway loss exists when it passes through such a channel. To study this type of flow, previous numerical works[3,4] were mostly focused on system level. They treated the inside of a filtration device as porous media and grossly estimate the ultra-filtration flow. However, for the design of a good filtration system, a study is still required to be detailed at fiber (or channel) level. Verma and Bhatt [5] previously in his work analytically described the flow within porous channels with the assumption that the suction and injection of the flow on the porous wall is uniform. However, this is not true in most of today's filtration processes. Qiu and Zhang's [6] and Damak et al.'s

* Corresponding author.
E-mail addresses: junfenglu@mail.ipc.ac.cn (J. Lu), luwq@gucas.ac.cn (W.-Q. Lu).

0017-9310/$ - see front matter © 2010 Elsevier Ltd. All rights reserved.
doi:10.1016/j.ijheatmasstransfer.2010.01.043

Nomenclature

C_b	solute concentration
C_M	mean solute concentration inside membrane pore
ΔC	trans-membrane concentration
d	the diameter of the pipe duct
D_s	solute diffusive coefficient
J_s	solute flux across membrane
J_v	ultra-filtration velocity
L_p	hydraulic permeability
P	hydraulic pressure
P_s	diffusive coefficient of the porous membrane
ΔP	trans-membrane pressure
r	solute radius
R	pore radius
R_{gc}	gas constant
S	solute generation source term on the membrane surface
T	absolute temperature
U^0	channel axis velocity
v_M	the flow rate on the surface of porous membrane
w	half-width of a channel
(u, v)	velocity vector
(x, y)	system coordinate
Δz	membrane thickness

Greek letters

μ	fluid viscosity
$\tau_{i,j}$	viscosity stress
ρ	density
σ	solute reflection coefficient

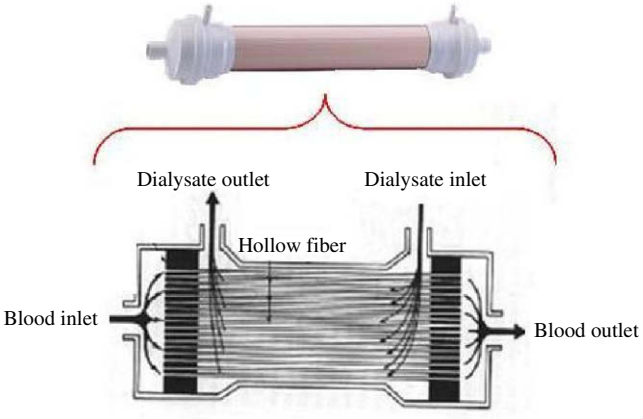

Fig. 1. Dialyzer.

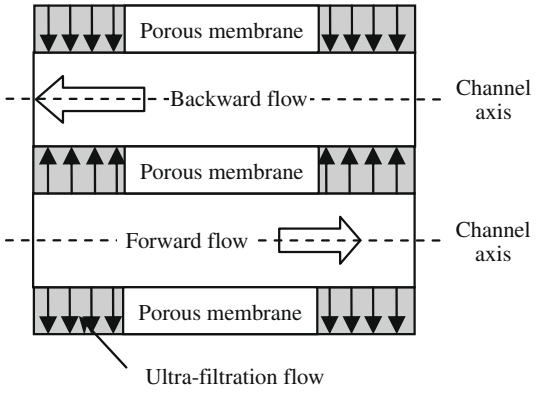

Fig. 3. Channel model.

[7] simulation works on ultra-filtration process only concerns one tubular flow with sideway ultra-filtration, and use Darcy's law to model trans-membrane ultra-filtration flow, but the pressure at the outside of the tube must be assumed during the simulation. Thus, till now, there is still not such a good simulation work which links the channel flow (both backward channel and forward channel in Fig. 3) and the ultra-filtration flow together because the boundary conditions on the membrane surface are hardly to be assumed.

As physical model used to interpret the fluid behavior when it passes through a semi-permeable membrane, Kedem–Katchalsky's (K–K) equations [8,9] were successfully used in a bunch of ultra-filtration processes. However, when the size of a flow reaches nano-scale, its behavior seems more ambiguous. The experimental work done by Gee et al. [10] showed that a thin liquid film (several

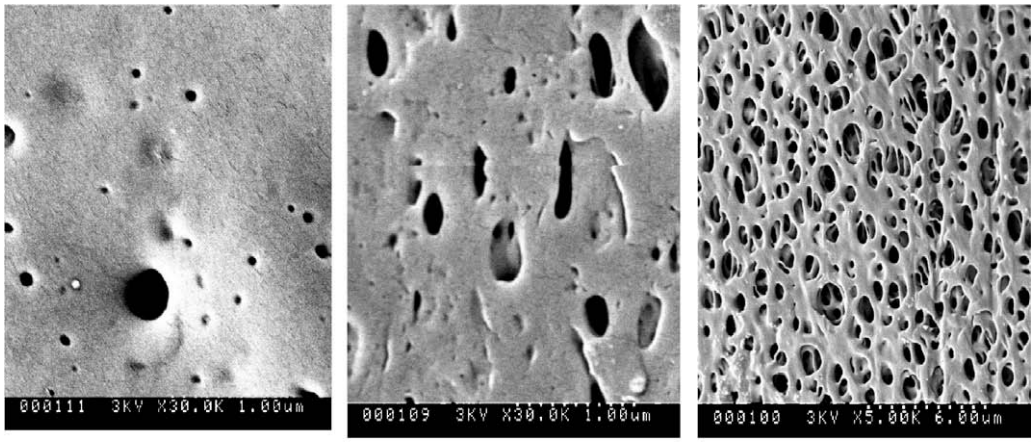

(a) PolyFlux 17S hollow fiber (polyarylethersulfone) at x30.0K

(b) SYNTRA 160 hollow fiber (polyethersulfone) at x 30.0 K.

(c) Optiflux hollow fiber (helixone) at x 5.0 K

Fig. 2. SEM images for different type of hemodialysis hollow fibers [1].

atomic layers) behaves like liquid crystals or ductile solids undergoing plastic deformation. This plastic behavior could cease a nano- or ultra- filtration process and further makes the K–K equations meaningless. Moreover, in the simulation work done by Thompson et al. [11], they found that slip boundary exists inside a thin channel with a size ranging from 16.71Ê to 24.57Ê (Ê ≈ characteristic molecular size), or <6 nm. Travis and Gubbins [12] had numerically simulated Poiseuille flow in long and narrow pore by non-equilibrium molecular dynamics method. The interaction potential between molecules is Lennard-Jones potential. Their results pointed out that when fluids is limited in the routeway of around 5 molecular diameters (around 1–2 nm), the flow cannot be described by Navier–Stokes equations. In most recent works [13,14], a MD (Molecular Dynamics) simulation is performed inside a nano-sized channel (around 3.4 nm). In the simulation, water (H_2O) was chosen as working fluid, and the channel was formed by alumina (Al_2O_3); when using thermal wall model [15], slip boundary was observed inside the channel, and the viscosity on the wall surface is also variable [13,14]. These results further lead to the variation of hydraulic permeability inside nano-sized pores of an ultra-filtration membrane. And this situation does not fit the primary condition that the hydraulic permeability of the K–K equations must maintain to be a constant value. The most recent MD simulation work [16] presented that the slip velocities on the wall boundaries were obviously observed when the channel size was below approximate 7.2 nm, and this size becomes a critical value for the slip phenomenon. Ziarani and Mohamad [17] had numerically simulated the flow of argon liquid in 7.32 nm channels by non-equilibrium molecular dynamics method. Week-Chandler–Anderson potential was employed to describe the interaction between two argon particles. In this work, they finally presented the good agreement of flow velocity field between analytic solution determined by Navier–Stoke's (N–S) equations and their MD results. Based on the above materials, for larger size permeating flow inside a nano-sized pore (dozens of nanometers), when the atomic level effects could be neglected, the flow is continuous and well coupled with N–S equations. In this case, the parameters (such as hydraulic permeability, diffusive coefficient, etc. (these parameters are based on continuum theory)) defined in the K–K equations are meaningful, thus, these equations could be used. Moreover, if one needs to use MD method to treat a permeating flow with a size of upper than 30 nm (millions of molecules), the design of mathematical models to transfer molecular level flow to bulk flow are further required, and this heavy task further needs the participation of huge parallel computers. This is not cost-effective. Thus, using K–K equations to approximately and fast model engineering ultra-filtration problems is better feasible when the size of permeating flow reaches dozens of nanometers [17].

To scrutinize a sort of mass transfer problems during the filtration process like hemodialysis, in this paper, numerical studies to analyze channel flow with sideway ultra-filtration are deployed at fiber level by using a specially designed "half-channel" model. To make the problem simple, only non-charged nano-sized substances carried by the fluid inside the channel are considered. The following sections detail the story.

2. Physical model

In this simulation, apparently, two levels of flows should be considered. Namely, the ultra-filtration flow and the channel flow.

2.1. Physical description of the ultra-filtration flow

The ultra-filtration flow passing through the porous membrane (Fig. 4) tends to be a little bit complicated. Typically, the physical phenomenon of a micro- or ultra-filtration process can be described by the following K–K equations:

$$J_v = L_p \cdot \Delta P - \sigma L_p R_{gs} T \cdot \Delta C \tag{1}$$

$$J_s = C_M(1-\sigma)J_v + P_s \cdot \Delta C \tag{2}$$

where L_p is hydraulic permeability of the porous membrane; ΔP is hydraulic pressure difference (or trans-membrane pressure) across the porous membrane; ΔC is solute concentration difference (or trans-membrane concentration) across the porous membrane; C_M is the mean solute concentration inside the pore of the porous membrane; J_v is ultra-filtration velocity or volumetric flux across the porous membrane; J_s is solute flux across the porous membrane; R_{gc} is gas constant, and T is absolute temperature; σ is solute reflection coefficient, as well P_s is diffusive coefficient of the porous membrane. In the above parameters, hydraulic permeability, reflection coefficient, and diffusive coefficient are three intrinsic ones. The relationship between σ, pore size, and particle size is described by Anderson's work [18,19]:

$$\sigma = \left(1 - \left(1 - \frac{r}{R}\right)^2\right)^2 \tag{3}$$

where r is the particle radius and R is the radius of pipe style pore. For small particles around 3 Å, when the pore size of the membrane is around 40 nm or more, σ is on the scale of 10^{-4}, which is very small. Thus, Eq. (1) can be further simplified to: ($L_p\Delta P \gg \sigma L_p R_{gc} T\Delta C$ in most cases)

$$J_v \approx L_p \cdot \Delta P \tag{4}$$

To determine the value of hydraulic permeability is a little bit tricky. In this paper, the pores of the membrane are assumed of pipe style. Furthermore, when considering non-charged solute particles inside the nano-sized pipe style pores, one can neglect the EDL (Electrical Double Layer) potential or Debye length [20,21] that influences the behaviors of ultra-filtration fluid inside these pores. With these specific assumptions, equations ever used in Brody et al.'s work [22] are introduced to calculate the hydraulic coefficient used in K–K equations with such condition: $D_s \gg Ru_{max}$ (the plug transport (Brody et al. [22, p. 3434]), where D_s is solute diffusive coefficient, typically, for small particles, its value is about 10^{-5} cm^2/s; R is the radius of the pore, u_{max} here is the maximum velocity of flow inside the pore). The equations are listed as follows (these equations were ever successfully used in micro-scale [22], and with previous assumption (non-charged solute particle), its survivability obviously could be extended to nano-scale):

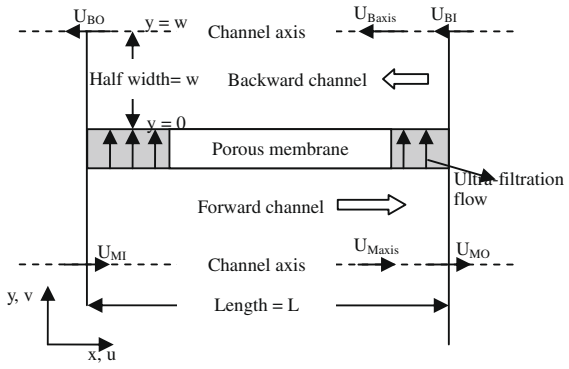

Fig. 4. Half-channel model.

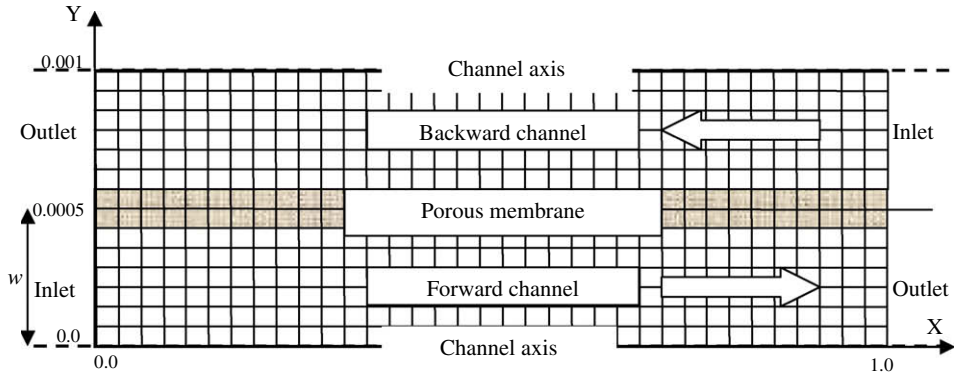

Fig. 5. Simulation mesh.

$$J_v(y) = \left(\frac{Gh^2}{12\mu}\right)\frac{96}{\pi^4}\sum_{i=1,3,5\ldots}^{\infty}\frac{1}{i^4}\left[1-\frac{\cosh(i\pi y/h)}{\cosh(i\pi h/2h)}\right] \quad \text{(Rectangular duct)} \quad -h/2 \leqslant y \leqslant h/2 \tag{5}$$

$$J_v(l) = \frac{G}{4\mu}\left(R^2 - l^2\right) \quad \text{(Pipe duct)} \tag{6}$$

$$G = -\frac{\partial P}{\partial z} = \frac{128\mu Q}{\pi d^4} \quad \text{(Poiseuille in pipe duct)} \tag{7}$$

where h, l, d, Q and μ are, respectively, the width or height of square duct, the range from the axis of the duct, the diameter of the pipe duct, the cross-sectional volumetric flow, and the viscosity of fluid in the duct; z is the axis direction of the duct.

When choosing a pipe duct as the model of the pore, L_p can be theoretically determined by the value of R. And then, with Eq. (4), one can get:

$$L_p \approx \frac{J_v}{\Delta P} = \frac{\overline{J_v(l)}}{(\Delta P/\Delta z)\cdot\Delta z} = \frac{1/(\pi R^2)\cdot\int_0^R J_v(l)2\pi\cdot l\,dl}{\partial P/\partial z\cdot\Delta z} = \frac{R^2}{8\mu\Delta z} \tag{8}$$

where Δz is the thickness of the membrane (or the length of the pore duct). Further more, assuming the porosity (the percentage of the pore area) of the porous membrane is M_p. Thus, L_p in Eq. (8) can be re-corrected as:

$$L_p \approx M_p\frac{R^2}{8\mu\Delta z} \tag{9}$$

At here, hydraulic permeability L_p of the porous membrane is theoretically determined. The only things left to be evaluated are C_M and P_s. P_s can be simply evaluated by the following equation [23]:

$$P_s = D_s M_p f \tag{10}$$

where f is the sieving coefficient of the membrane, for straight channel style pore, $f \approx 1$.

To determine C_M, the distribution of solute concentration inside a straight channel pore should be obtained. This was analytically solved by Crank [24]. The equation is listed as follows:

$$C(x,t) = \frac{C_0}{2}\left\{1+\left[\operatorname{erf}\frac{x}{2\sqrt{D_s\cdot t}} + \exp(hx+h^2D_s t)\times\left(1-\operatorname{erf}\left(\frac{x}{2\sqrt{D_s\cdot t}}+h\sqrt{D_s\cdot t}\right)\right)\right]\right\} \tag{11}$$

$$h = 2\frac{P_s}{D_s\Delta Z}$$

Since the simulation in this work is performed in steady state, removing the time dependent terms in Eq. (11) one can get the mean solute concentration C_M inside a straight channel by integration as:

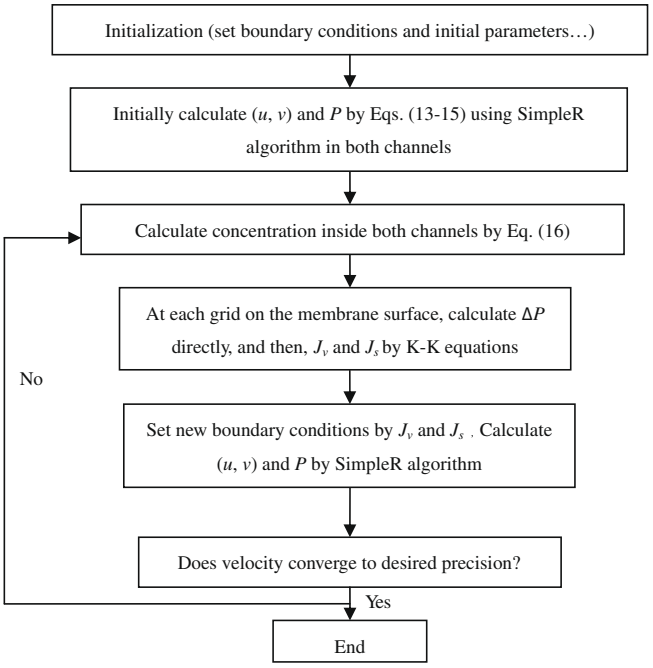

Fig. 6. Iteration diagram.

$$C_M = \frac{1}{\Delta Z}\int_0^{\Delta Z} c(x)\,dx = \frac{1}{\Delta Z}\int_0^{\Delta Z}\frac{C_0}{2}(1+\exp(hx))\,dx = \frac{C_0}{2}\left(1+\frac{\exp(h\Delta Z)-1}{h\Delta Z}\right) \tag{12}$$

2.2. Physical description of the channel flow

In general, considering steady incompressible Newtonian fluid, the flow inside the channel is governed by the Navier–Stokes equations listed as follows:

Continuity equation

$$\frac{\partial u}{\partial x}+\frac{\partial v}{\partial y} = 0 \tag{13}$$

Momentum equation

$$u\frac{\partial u}{\partial x}+v\frac{\partial u}{\partial y} = -\frac{1}{\rho}\frac{\partial P}{\partial x}+\frac{1}{\rho}\left(\frac{\partial\tau_{11}}{\partial x}+\frac{\partial\tau_{21}}{\partial y}\right) \tag{14}$$

$$u\frac{\partial v}{\partial x}+v\frac{\partial v}{\partial y} = -\frac{1}{\rho}\frac{\partial P}{\partial y}+\frac{1}{\rho}\left(\frac{\partial\tau_{22}}{\partial x}+\frac{\partial\tau_{12}}{\partial y}\right) \tag{15}$$

Table 1
Simulation conditions.

Channel parameters	
Height	0.001 m
Length	1 m
Solute particle size (r)	0.3 nm
Wall porosity(M_p)	30%
Pore size (R)	40 nm, 50 nm, 60 nm, 70 nm, 80 nm
Solute diffusive coefficient (D_s)	1E−5 cm^2/s
Diffusive coefficient of the porous membrane (P_s)	3E−6 cm^2/s
Viscosity (μ)	
Forward channel	4.7E−3 kg/(m s)
Backward channel	1.1E−3 kg/(m s)
Density (ρ)	
Forward channel	1.05E+3 kg/m^3
Backward channel	1.01E+3 kg/m^3
Axis velocity ($U_{l,O}$)	
Forward channel inlet	1.67 mm/s
Backward channel inlet	2.78 mm/s
Initial pressure settings	
Forward channel inlet	125 mmHg
Backward channel outlet	115 mmHg
Initial solute concentration	
Forward channel inlet	10 mg/dL
Backward channel inlet	0

Table 2
Hydraulic coefficients (L_p) with membrane porosity M_p = 0.3

Pore size (nm)	L_p (10^{-10} m/s/Pa)
40	0.83
50	1.29
60	1.86
70	2.53
80	3.31

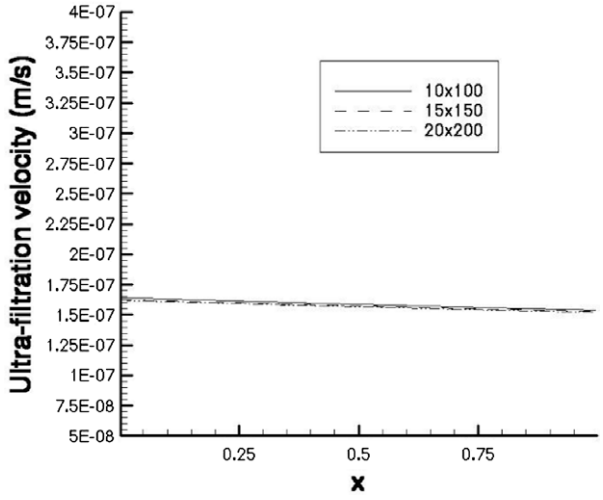

Fig. 7. Comparison of the ultra-filtration results for different mesh schemes.

where (u, v) is velocity vector; P is hydraulic pressure; ρ is fluid density; τ_{ij} is viscosity stress.

Concentration equations

The solute concentration inside either forward channel or backward channel can be governed by the following equation:

$$u\frac{\partial C_b}{\partial x}+v\frac{\partial C_b}{\partial y}=D_S\left(\frac{\partial^2 C_b}{\partial x^2}+\frac{\partial^2 C_b}{\partial y^2}\right)+S \tag{16}$$

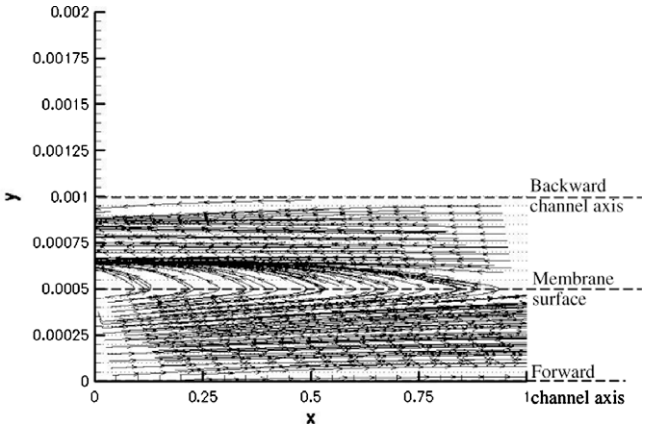

Fig. 8. Channel velocity stream lines (pore size = 90 nm).

where C_b is the solute concentration, D_s is solute diffusive coefficient, (u, v) is the flow velocity vector inside the channel, S is solute generation source term on the membrane surface. Apparently, the following two redundant equations (these two equations link the volume flow and solute relations between two channels) are also useful:

$$S=J_s/\Delta x \tag{17}$$

$$v_M=J_v \tag{18}$$

where Δx is unit length of the porous membrane; v_M is the flow rate on the surface of porous membrane (On the membrane surface, considering non-slip condition, obviously, the velocity component in the "x"-direction is zero. And this perpendicular component (v_M) is just the ultra-filtration flow rate). Holding Eqs. (17) and (18), one can solve (13)–(16) by iteration.

2.3. Simulation algorithm and conditions

A three-layer mesh (meshes set on backward channel, membrane and forward channel) used in the simulation is designed as shown in Fig. 5. Boundary conditions at the channel axis are listed as follows:

$$v=0,\quad \frac{\partial v}{\partial x}=0,\quad \frac{\partial^2 v}{\partial x^2}=0,\quad \frac{\partial u}{\partial y}=0,\quad \frac{\partial P}{\partial y}=0,\quad \frac{\partial C}{\partial y}=0 \tag{19}$$

Neglecting the tiny sideway ultra-filtration along the membrane, the shape of frontier profile of the Newtonian channel flow should be parabolic, thus, the inlet or outlet velocity profiles of both channels are considered parabolic:

$$u(y)=c_0y^2+c_1y+c_2 \tag{20}$$

where, specifically, in the forward channel:

$$c_0=-\frac{U^0}{w^2},\quad c_1=0,\quad c_2=U^0$$

and in the backward channel:

$$c_0=-\frac{U^0}{w^2},\quad c_1=\frac{4U^0}{w},\quad c_2=-3U^0$$

where U^0 is the axis velocity, w (= 0.0005 m) is the half-width of the channel.

The flows inside the forward channel and backward channel are connected by Eqs. (1), (17) and (18), and simulated by using the famous "SimpleR" algorithm [25]. The iteration algorithm is listed in Fig. 6.

Table 1 lists initial conditions of the simulation. Table 2 lists the hydraulic coefficients determined by Eq. (9) used in the simulation.

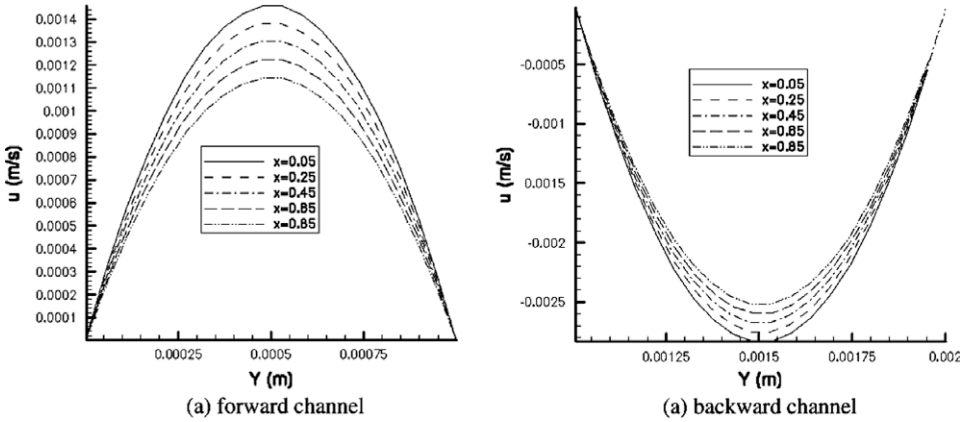

Fig. 9. Normalized frontier velocity profile inside channels (membrane pore size = 50 nm).

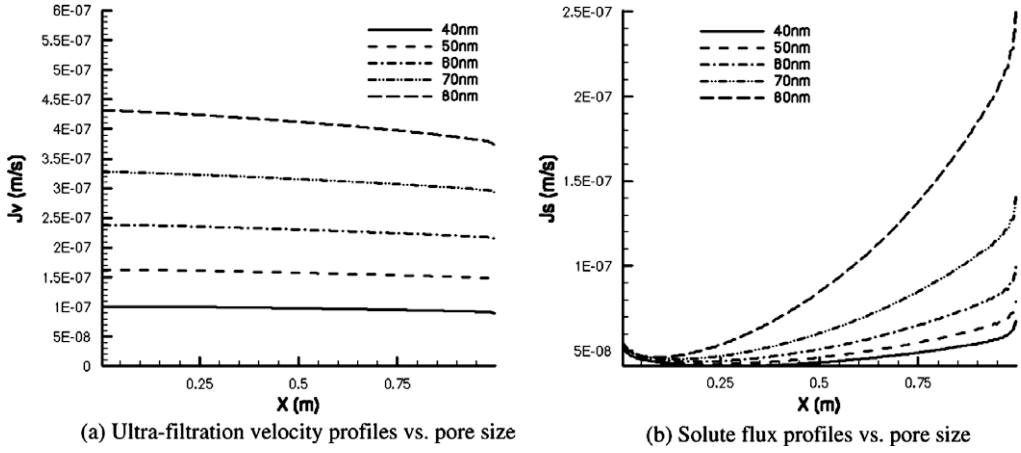

Fig. 10. Ultra-filtration velocity and solute flux profiles along membrane surface.

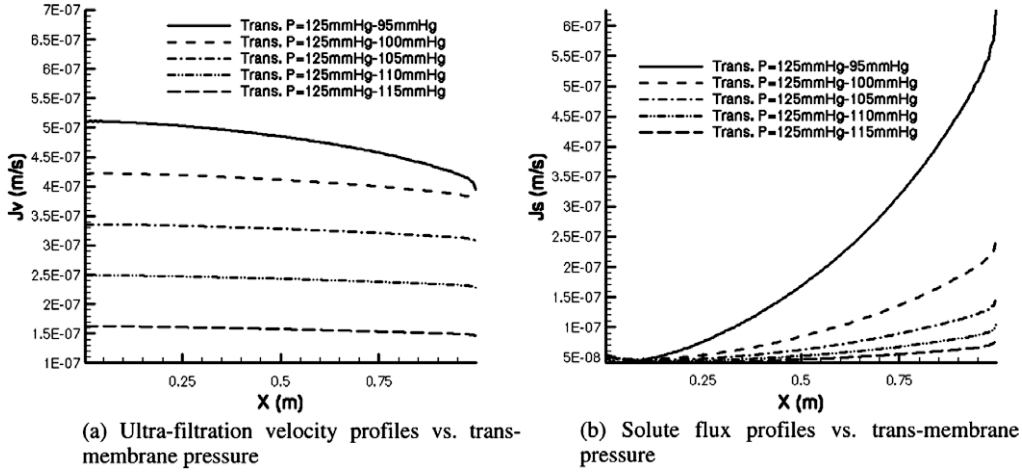

Fig. 11. Ultra-filtration velocity and solute flux profiles with different trans-membrane pressure.

3. Simulation results and discussion

Initially, the grid independence of the mesh scheme is required to be tested. The ultra-filtration velocities have been obtained on the meshes of 10×100, 15×150, and 20×200, respectively, in Fig. 7. The results of different meshes are all well fitted in the figure. In the following, 15×150 mesh in each half-channel is chosen in calculation.

The velocity stream lines at both channels are shown in Fig. 8. In the figure, the stream lines that link the flow between forward channel (lower part) and backward channel (upper part) are where the ultra-filtration flow passes through. And these lines are densely distributed in the outlet area of backward channel, because the ultra-filtration flow rate is much higher at this area owning to the preset higher trans-membrane pressure.

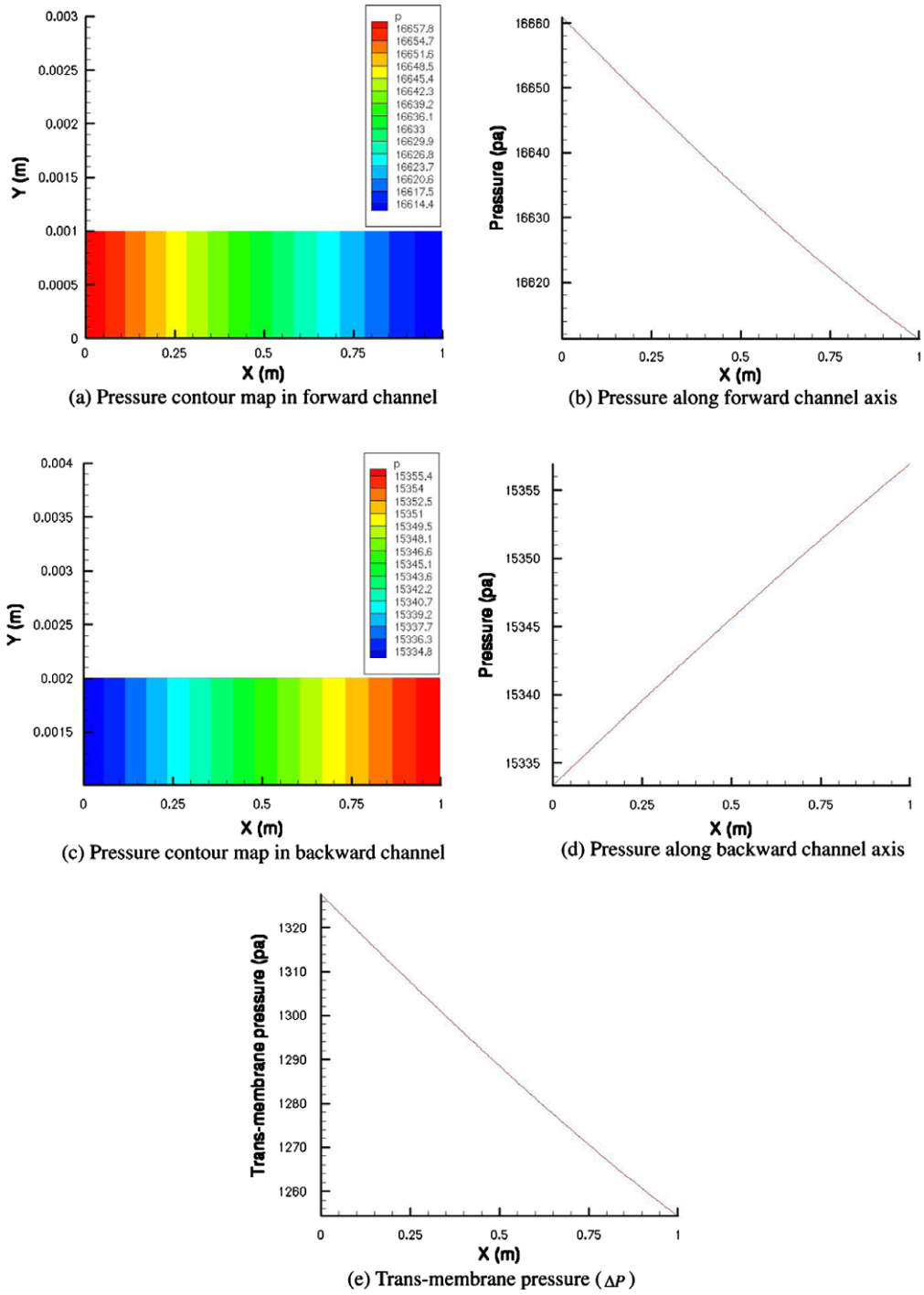

Fig. 12. Pressure (pore size = 50 nm).

Fig. 9 shows the frontier velocity profiles inside two channels. In this figure, one can find that the velocity profiles along *x*-direction in both forward channel and backward channel are nearly in parabolic shape. And the profiles are falling down in the forward channel along *x*-direction, and rising in the backward channel. The falling or rising of the parabolic shape is just caused by the sideway ultra-filtration loss.

Fig. 10(a) shows the profiles of ultra-filtration velocity (J_v) along the porous membrane surface simulated in different pore sizes (pore size = 40, 50, . . ., 80 nm) of the membrane. In general, the profiles are falling down from the inlet of the forward channel to its outlet. The larger the pore size of the porous membrane, the more the ultra-filtration velocity sideway loss in the forward channel. Because of miner pressure expense inside the channels, even at the outlet of the forward channel, the pressure of the forward channel is still much greater than that of backward channel. This produces the positive ultra-filtration velocities along the whole porous membrane. The profiles of solute flux (J_s) along the membrane surface are shown in Fig. 10(b). Apparently in the figure, larger pore size of the membrane also produces more amount of solute throughput. The uplifting shape of the profile tells that, if the pore size is fixed, the solute flow is more influenced by the trans-membrane concentration (ΔC)

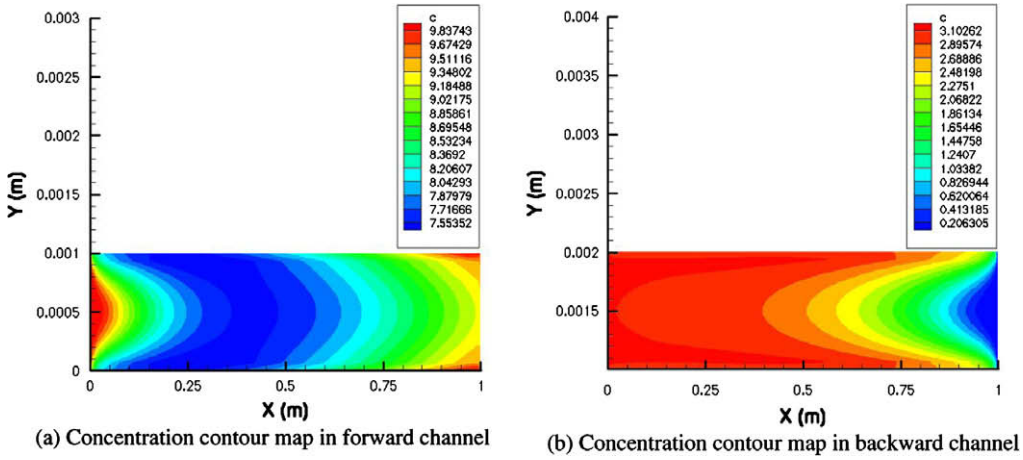

Fig. 13. Concentration contour map (pore size = 50 nm, the unit of concentration is "mg/dL").

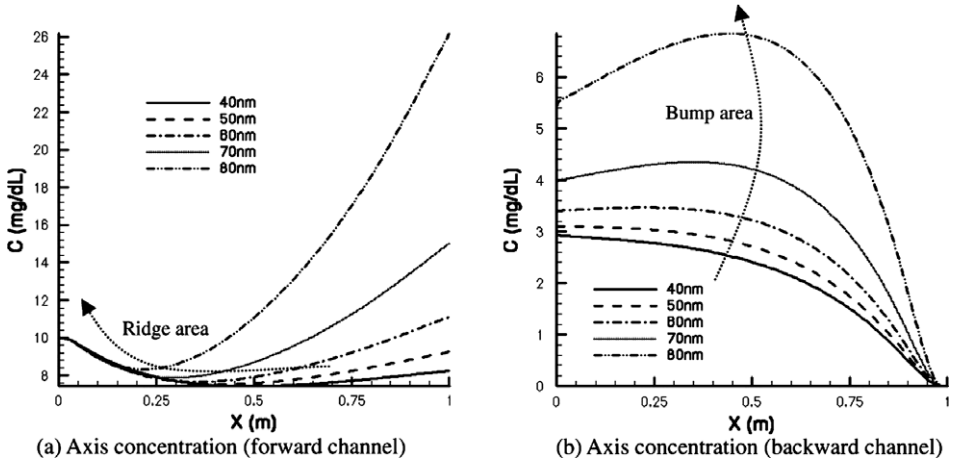

Fig. 14. Axis concentration comparison.

between the two channels, but not J_v (because J_v is falling along the channel Fig. 10(a)) (see Eq. (2)). This uplifting route also indicates that the trans-membrane concentration (ΔC) at the outlet area of forward channel is much higher than that at the inlet area.

In Fig. 11(a), one can see that when the initial pressure settings are modified, the ultra-filtration curve also moves accordingly. The more the trans-membrane pressure (= forward channel inlet pressure − backward channel outlet pressure), the higher the location of the curve. More trans-membrane pressure also causes more amount of ultra-filtration, thus further increases the throughput of solute (Fig. 11(b)).

Owning to the small amount of ultra-filtration flow permeating through the porous membrane, the pressure drop per unit length inside each channel almost maintains in a constant value (see Fig. 12(a)–(d)). The sideway pressure loss from each channel axis to the membrane surface is minor (Fig. 12(a) and (c)). From this, one can also deduce that the trans-membrane pressure can be further calculated by:

$$\Delta P \approx P_{\text{forward\_channel\_axis}} - P_{\text{backward\_channel\_axis}} \tag{21}$$

Since the pressure along the axis of each channel is nearly linear (Fig. 12(b) and (d)), the trans-membrane pressure produced by Eq. (21) is also nearly linear (Fig. 12(e)). This finally results in a nearly linear ultra-filtration velocity profile along the membrane surface (Eq. (4)).

Fig. 13 shows the solute concentration contour map inside the double channels. The shape of the contour profile indicates that, in general, the solute concentration decreases from the channel axis to the membrane surface. The concentration contour in the forward channel (Fig. 13(a)) is initially falling down to its ridge from inlet area to the halfway of the channel. And then, it heads up to the outlet of the channel. In the backward channel (Fig. 13(b)), the concentration contour does not contain a ridge, and it uplifts to the outlet of the channel. To scrutinize this interesting property, the axis concentrations are outlined in Fig. 14. In forward channel (Fig. 14(a)), the ridge area is moving to the left when the pore size is enlarged. This phenomenon is caused by two counteracting mechanisms: (1) the sideway leakage of volume flow which leads the increase of solute concentration in the channel; (2) the sideway loss of solute which tends to decrease solute concentration in the channel. Fig. 10 tells that J_v is much larger than J_s if the pore size is fixed. This indicated that the first mechanism is strong in the forward channel. And when the pore size is enlarged, this mechanism is even stronger to drag the ridge area to the inlet area (labeled by dashed arrow in Fig. 14(a)). The solute concentrations distributed at the axis of the backward channel are also outlined in Fig. 14(b). In general, the concentration is climbing from inlet of backward channel to its outlet. Comparing with the ridge area in Fig. 14(a), there is clearly a bump area inside each curve. The bump is mostly generated by the speed-up velocity of J_s accompanied by the enlargement of the membrane pore size. From Fig. 11(a), one can find that when

the pore size increases, the slope of the J_v curve increases slightly, meanwhile, the speed of J_s increase dramatically especially at the outlet area of the forward channel (Fig. 11(b)). Since the flow of the backward channel runs reversely, the bump on the concentration curve is finally squeezed out.

In the process of ultra-filtration, normally, the flows in those two channels run oppositely. This could cause a big difference of trans-membrane pressure between the left site and the right site of the porous membrane, and further lead to the unbalanced ultra-filtration on the membrane surface. In the medical process of hemodialysis, such unbalanced ultra-filtration profile is a cause of pore clogging problem of a filtration membrane. This problem will further increase the expense from the patient on hemodialyzers. Thus, in this sort of filtration processes, uniform ultra-filtration pattern across membrane is highly preferred. To simulate this, supposing that flow either in the forward channel or backward channel runs in the same direction, also, at the same time, nearly same initial pressure gradient both in the forward channel and backward channel is set, more specifically, let:

Table 3
Initial conditions

Pore size (R)	100 nm
Pressure	
Forward channel inlet	125 mmHg
Backward channel inlet	100 mmHg

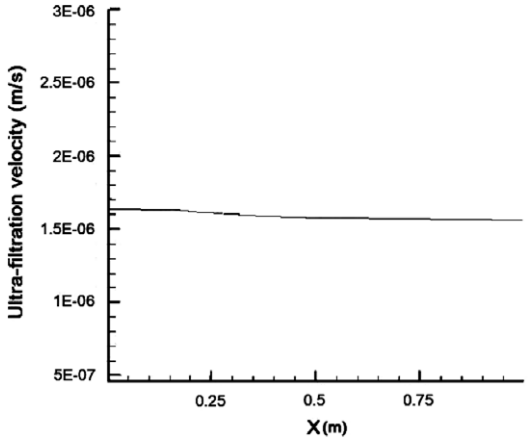

Fig. 15. Ultra-filtration profile along channel wall surface (pore size = 100 nm).

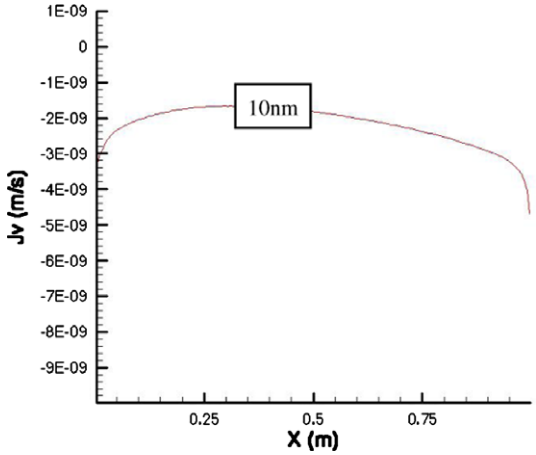

Fig. 16. Back-filtration caused by small pore size.

$$P_{\text{Backwardchannel\_inlet}} - P_{\text{Backwardchannel\_outlet}} \approx P_{\text{Forwardchannel\_inlet}} - P_{\text{Forwardchannel\_outlet}} \quad (22)$$

With initial conditions list in Table 3, a special case (the flows both in the forward channel and in the backward channel run in the same direction) for the ultra-filtration profile along the membrane surface is simulated. Near uniformly distributed ultra-filtration velocity profile was formed as shown in Fig. 15. The variation of ultra-filtration is within ±3.0E−8 m/s, which is much smaller than that of ultra-filtration rate (1.6E−6 m/s).

Back-filtration problem [26–28] is a critical issue during the process of hemodialysis, because it induces the contamination of the blood. Typically, this sort of problems is mostly caused by local variation of trans-membrane pressure, and the negative trans-membrane pressure mostly at the blood outlet area of the dialyzer because of the blood pressure loss through the hollow fiber pathway. However, in some case, when the pore size of the membrane is very small, even the pressure in the whole blood channel (forward channel) is higher than that in the dialysate channel (backward channel), this sort of problem could also be happening. To explain this, a case (pore size = 10 nm) with non-charged particles is simulated as shown in Fig. 16. In this case, the back-filtration problem comes from reverse osmosis instead of negative trans-membrane pressure. In this figure, $J_v < 0$ (or from Eq. (1): $\Delta P < \sigma R_{gc} T \Delta C$) in the whole channel. Or, physically speaking, the hydraulic trans-membrane pressure could not overcome the trans-membrane osmotic pressure, thus reverse osmosis happens.

4. Conclusion

By taking a unique "half-channel" model, this paper details a sort of ultra-filtration problems by numerical simulation. The novelty of this paper is that, by the utilization iteration algorithm used in Fig. 6, the pressure under or above the porous membrane does not need to be artificially given because "SimpleR" algorithm fixed it at each channel during each iteration (before this work the trans-membrane pressure must be assumed [6,7]). The effects of pore size and trans-membrane pressure on ultra-filtration velocity J_v and solute flux J_s through the membrane are depicted in detail. The concentration and pressure contours in the channel, as well as channel axis concentration profiles are detailed and analyzed. Concentration ridge and bump phenomena induced by the size effect of the membrane pore were observed, respectively, in forward and backward channels. These phenomena also reveal the dilution and accumulation of solutes inside channels. And these results could further provide hints to engineers for their design of better filtration system. Moreover, a practical suggestion for the hemodialysis process is put forward telling that during the process, in order to improve the membrane utilization, the trans-membrane pressure should be uniquely set (Eq. (22)), and the applied flows in both channels should run in the same direction. Finally, the simulating result at 10 nanometer aperture shows that a back-filtration caused by reverse osmosis occurs.

Acknowledgement

This work is partially supported by NSFC fund (No. 50776095).

References

[1] Z.P. Huang, A study of novel and optimal technology for hemodialysis, Ph.D. Thesis, University of Kentucky, Lexington, Kentucky, 2003.
[2] C.K. Poh, J.F. Lu, W.R. Clark, D.Y. Gao, Kidney artificial, Encycl. Biomater. Biomed. Eng. (2006), doi:10.1081/E-EBBE-120007344.

[3] W.P. Ding, L.Q. He, G. Zhao, Z.Q. Shu, S.X. Cheng, D.Y. Gao, A novel mass transfer theoretical model used in hollow fiber dialyzer, Chin. Sci. Bull. (Chinese version) 48 (15) (2003) 1642–1646.
[4] Z.J. Liao, Numerical and experimental study of mass transfer in the artificial kidney and hemodialysis, Doctor Dissertation, College of Engineering at the University of Kentucky, 2002.
[5] P.D. Verma, B.S. Bhatt, Laminar flow through parallel and uniformly porous walls of different permeability, Indian J. Phys. 47 (1973) 718–728.
[6] Y.R. Qiu, Q.X. Zhang, Mass transfer mathematical model for one-side plate steady-state ultrafiltration, Trans. Nonferrous Met. Soc. China 15 (3) (2005) 686–690.
[7] K. Damak, A. Ayadi, B. Zeghmati, P. Schmitz, A new Navier–Stokes and Darcy's law combined model for fluid flow in cross-flow filtration tubular membranes, Desalination 161 (2004) 67–77.
[8] O. Kedem, A. Katchalsky, Thermodynamic analysis of the permeability of biological membranes to non-electrolytes, Biochem. Biophys. Acta 27 (1958) 229–246.
[9] O. Kedem, A. Katchalsky, A physical interpretation of the phenomenological coefficients, J. Gen. Physiol. 45 (1961) 143–179.
[10] M.L. Gee, P.M. McGuiggan, J.N. Israelachvili, Liquid to solid-like transitions of molecularly thin films under shear, J. Chem. Phys. 93 (3) (1990) 1895–1906.
[11] P.A. Thompson, S.M. Troian, A general boundary condition for liquid flow at solid surfaces, Nature 389 (1997) 360–362.
[12] K.P. Travis, K.E. Gubbins, Poiseuille flow of Lennard-Jones fluids in narrow slit pores, J. Chem. Phys. 112 (2000) 1984–1994.
[13] Y. Chu, J.F. Lu, W.Q. Lu, Molecular dynamics simulation of fluid transport in nanoscale pore of porous medium, in: Proceedings of the Sixth International Symposium on Multiphase Flow, Heat Mass Transfer and Energy Conversion, Paper No. MN-54, Xi'an, China, 2009.
[14] Y. Chu, J.F. Lu, W.Q. Lu, Numerical simulation of fluid Transport in a single micro-nano pore of porous membrane, in: ASME Paper HT09-88354, ASME 2009 Summer Heat Transfer Conference, San Francisco, USA, 2009.
[15] R. Tehver, F. Toigo, J. Koplik, J.R. Banavar, Thermal walls in computer simulations, Phys. Rev. E 57 (1998) R17–R20.
[16] J.F. Lu, Y. Chu, W.Q. Lu, An investigation for the usability of K–K equations for nano porous membranes, in: ASME Paper MNHMT2009-18088, ASME 2009 Second Micro/Nanoscale Heat & Mass Transfer International Conference, Shanghai, China, 2009.
[17] A.S. Ziarani, A.A. Mohamad, A molecular dynamics study of perturbed Poiseuille flow in a nanochannel, Microfluid. Nanofluid. 2 (2005) 12–20.
[18] L. Anderson, M. Malone, Mechanism of osmotic flow in porous membranes, Biophys. J. 14 (1974) 957–983.
[19] L. Anderson, Configurational effect on the reflection coefficient for rigid solutes in capillary pores, J. Theor. Biol. 90 (1981) 405–426.
[20] R. Qiao, N.R. Aluru, Transient analysis of electroosmotic flow in nano diameter channels, in: Technical Proceedings of the 2002 International Conference on Modeling and Simulation of Microsystems, Nanotech 2002, vol. 1, pp. 28–31, 2002.
[21] S. Ghosal, Z. Lu, 2002, Electroosmotic flow and zone broadening in microfluidic channels of variable cross-section and wall charge, in: Technical Proceedings of the 2002 International Conference on Modeling and Simulation of Microsystems, Nanotech 2002, vol. 1, pp. 68–71.
[22] J.P. Brody, P. Yager, E.G. Raymond, R.H. Austin, Biotechnology at low Reynolds numbers, Biophys. J. 71 (1996) 3430–3441.
[23] M. Marucci, S.G. Pettersson, G. Ragnarsson, A. Axelsson, Determination of a diffusion coefficient in a membrane by electronic speckle pattern interferometry: a new method and a temperature sensitivity study, J. Phys. D: Appl. Phys. 40 (2007) 2870–2880.
[24] J. Crank, The Mathematics of Diffusion, second ed., Oxford University Press, Oxford, 1975.
[25] S.V. Patankar, A calculation procedure for two-dimensional elliptic situations, Numer. Heat Transfer 4 (1981) 409–425.
[26] U. Baurmeister, M. Travers, J. Vienken, G. Harding, C. Million, E. Klein, T. Pass, R. Wright, Dialysate contamination and back filtration may limit the use of high-flux dialysis membranes, ASAIO Trans. 35 (3) (1989) 519–522.
[27] V. Panichi, S. De Pietro, B. Andreini, M. Migliori, V. Tessore, D. Taccola, P. Rindi, R. Palla, C. Tetta, Cytokine production in haemo diafiltration: a multicentre study, Nephrol. Dial. Transplant. 13 (7) (1998) 1737–1744.
[28] M. Mineshima, I. Ishimori, T. Akiba, Estimation of back filtration flow rate in commercially available high flux dialyzers: importance of water purification system for dialysate, Hemodial. Int. 9 (1) (2005) 75–76.